

# Enabling Indoor Mobile Millimeter-wave Networks Based on Smart Reflect-arrays

Xin Tan<sup>1</sup>, Zhi Sun<sup>1</sup>, Dimitrios Koutsonikolas<sup>2</sup>, and Josep M. Jornet<sup>1</sup>

<sup>1</sup>Department of Electrical Engineering, <sup>2</sup>Department of Computer Science and Engineering  
State University of New York at Buffalo, Buffalo, NY 14260

E-mail: {xtan3, zhisun, dimitrio, jmjornet}@buffalo.edu.

**Abstract**—The millimeter-wave (mmWave) frequency band has been utilized in the IEEE 802.11ad standard to achieve multi-Gbps throughput. Despite the advantages, mmWave links are highly vulnerable to both user and environmental mobility. Since mmWave radios use highly directional antennas, the line-of-sight (LOS) signal can be easily blocked by various obstacles, such as walls, furniture, and humans. In the complicated indoor environment, it is highly possible that the blocked mmWave link cannot be restored no matter how the access point and the mobile user change their antenna directions. To address the problem and enable indoor mobile mmWave networks, in this paper, we introduce the reconfigurable 60 GHz reflect-arrays to establish robust mmWave connections for indoor networks even when the links are blocked by obstructions. First, the reconfigurable 60 GHz reflect-array is designed, implemented, and modeled. Then a three-party beam-searching protocol is designed for reflect-array-assisted 802.11ad networks. Finally, an optimal array deployment strategy is developed to minimize the link outage probability in indoor mobile mmWave networks. The proposed solution is validated and evaluated by both in-lab experiments and computer simulations.

## I. INTRODUCTION

The usage of millimeter-wave (mmWave) frequency bands has significantly facilitated the next generation wireless communications. In the IEEE 802.11ad standard, the 2.16 GHz bandwidth around 60 GHz can dramatically address the current spectrum shortage in the busy 5GHz/2.4GHz Wi-Fi frequency band [1]–[5]. The millimeter scale signal wavelength enables very small antenna arrays in both access point (AP) and the mobile user devices [6] that provide highly efficient directional transmissions. The huge bandwidth and the directional transmissions can achieve the data rates of up to 6.7 Gbps in an indoor WLAN setting [7].

Despite the advantages, mmWave wireless transmissions suffer from much higher path loss due to the Friis' Law [8]. Therefore, directional antennas, e.g., horn antennas or antenna arrays, are used to form narrow transmission beams to compensate the high path loss. While the quasi-optical propagation characteristics of mmWave transmission are suitable for fixed line-of-sight (LOS) links, such links can be easily broken due to user mobility and the obstacles in the environment. Due to the narrow beamwidth of mmWave signals, the misalignment of the TX and RX antennas can significantly reduce the antenna gain, while a very small obstacle, such as a person's arm, can effectively block the link [9]–[12].

<sup>†</sup> This work was supported by the US National Science Foundation (NSF) under Grants No. CNS-1629929 and No. CNS-1553447.

For the broken mmWave link due to misalignment, existing beam-searching solutions for IEEE 802.11ad networks can be used to change the direction of the TX and RX beams to re-establish the antenna alignment and restore the link [13]–[15]. However, for the broken mmWave link due to the obstruction blockage, changing the antenna direction alone is not enough to repair the link, especially in indoor environments. First, the dielectric materials in the indoor environment, such as concrete walls, doors, furniture, and people themselves, can easily create blockage to the LOS mmWave link, which cannot be restored by simply changing the TX or RX antenna direction. Second, if the indoor environment does not have sufficient metallic surfaces, there is no reflected link that can be used to connect the AP and the mobile user. On the one hand, a few metallic surfaces can only form a very limited number of reflected paths that have fixed incident and reflected angles, which have very limited effects on reducing the area blocked by obstacles. On the other hand, other dielectric objects, e.g., walls and furniture, are bad at reflecting mmWave signals.

In this paper, to address the aforementioned link blockage problem, we propose to deploy smart reflect-arrays in the indoor environment that can adaptively establish robust mmWave connection when the LOS path and non-LOS paths with natural reflections are blocked by obstructions. The proposed mechanism is compatible with the IEEE 802.11ad protocol and can greatly enhance the mmWave link robustness when a user devices move in the complicated indoor environment. Our objective is to minimize the link outage probability when user device is randomly moving in an indoor environment with various obstacles, incorporating the antenna sector selection at the AP and mobile user as well as the configuration of the smart reflect-arrays. Specifically, our contributions can be summarized as follows.

First, a smart reflect-array-assisted mmWave network system is proposed for the first time. As shown in Fig. 1, by deploying the passive and electronically reconfigurable reflect-array at appropriate positions in the indoor environment, the incident signal from the 802.11ad AP can be steered towards the mobile user that is blocked by any obstacles. It should be noted that existing solutions to signal blockage using active relay nodes, such as the mmWave virtual reality (VR) system in [12], have to either compromise the data rate by using half a duplex scheme or suffer from self-interference in the full-duplex mode. In contrast, the proposed reflect-array-assisted system is completely passive and can achieve full duplex

relaying without any self-interference. Hence, the transmission rate is not affected. Furthermore, the VR system in [12] uses laser trackers to locate the user in real time. However, for other devices, such as phones and laptops, additional hardware and software are required to accurately track their positions in real time. In contrast, the proposed reflect-array-assisted mmWave network uses beam-searching method to find the optimal beam direction for desired users, which does not need any location information.

Second, we design and implement a 60 GHz reflect-array that consists of 224 reconfigurable patches. Different from the natural reflection utilized in [16], the reflection coefficient of each patch can be electronically controlled in real time so that the direction of the reflected signal can be arbitrarily controlled. Although the idea of a 60 GHz reflect-array has been introduced in [17], it was used as part of the TX or RX antenna to enable beamforming. In contrast, the reflect-array used in this paper is placed in the middle of the mmWave channel to change the direction of propagation of mmWave signals. The implementation cost of the reflect-array designed in this paper is also much lower since relay switches are used in stead of p-i-n diodes to control the reflector units. In addition, the reconfigurable reflection coefficient and beamforming performance of the proposed reflect-array are also theoretically modeled to facilitate the optimal protocol design.

Third, a three-party beam-searching protocol is designed for the smart reflect-array-assisted 802.11ad networks. Different from existing beam searching protocols used in mmWave networks that only involve the antenna sector selection of the TX and RX node [18], [19], the proposed system introduces the third party, i.e., the reflect-array, which can also be controlled to steer the signal propagation direction. The developed three-party beam-searching protocol supports plug-and-play for 802.11ad networks without changing the existing protocol in the transceivers.

Fourth, an optimal array deployment strategy is developed to minimize the link outage probability in indoor mobile mmWave networks. We consider an arbitrary indoor environment with various obstacle distribution. While the AP position is fixed, the movement of user devices follows the “random mobility model” [20]. We formulate the optimal array deployment as a geometric overlap problem, which is solved by the exhaustive method by considering the limitation of indoor constructions in the real case.

The remainder of the paper is organized as follows. In Section II, we introduce the system architecture, the experimental test-bed, and the experimental result for the reflect-array-assisted 802.11ad networks. The beam-searching algorithm is developed in Section III. Then, the deployment of the reflect-arrays is optimized in Section IV. The numerical analysis of the link outage probability is presented in Section V. Finally, the paper is concluded in Section VI.

## II. REFLECT-ARRAY DESIGN AND PROOF-OF-CONCEPT EVALUATION

In this section, we first describe the system architecture of the reflect array-assisted 802.11ad networks. Then, we discuss

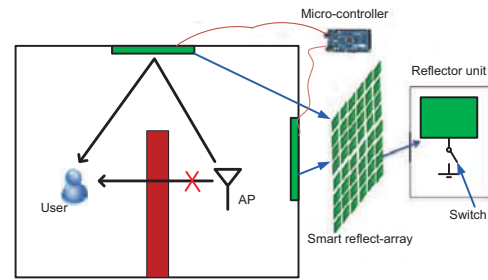


Fig. 1. The system architecture.

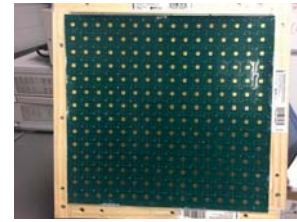


Fig. 2. The smart reflect-array panel.

the design and implementation of the reflect-array and use test-bed experiments to prove the feasibility of the proposed solution.

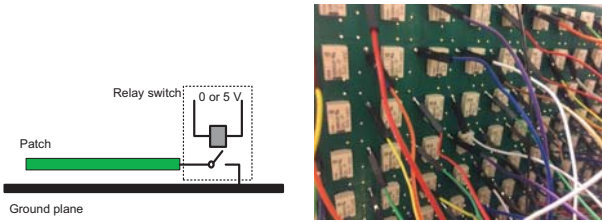
### A. System Architecture

The system architecture is illustrated in Fig. 1. The AP and the user are deployed in the indoor environment. According to the IEEE 802.11ad protocol, the AP performs the beam-searching to maintain a connection with the mobile user. However, due to the obstacle between the AP and user, the LOS path is blocked and communication cannot be established in this case.

Once an outage occurs for the LOS link, the reflect-array hung on the wall establishes the communication links using the controlled reflected path to bypass the obstacle. The reflect-array consists of a cluster of small patch reflectors and the micro-controller is used to control the electromagnetic response of each reflector. During the beam-searching period of the IEEE 802.11ad protocol, the reflect-array receives the signal from the AP and then steers it towards the desired user based on the control algorithm. Different from existing MIMO, beamforming, or active relay techniques, the proposed smart reflect-array just reflects the incident signal and steers it to the user in a passive way. Therefore, the proposed system helps transceivers to establish extra reflect-path links without any change in hardware of the AP and client. Moreover, different from the existing active relay-based solutions, the proposed reflector array-based solution does not suffer from self-interference when relaying signals in the full-duplex mode.

### B. Design and Implementation of the Reflect-array

As shown in Fig. 2, the reflector panel is fabricated with RTduroid 5880 high frequency laminates with a dielectric constant of 2.2 and a dissipation factor of 0.0009. The dimension of the panel is 337 mm × 345 mm × 0.254 mm



(a) The switch loaded on the patch (b) The switches soldered on the panel.

Fig. 3. The relay switches for reflector units control.

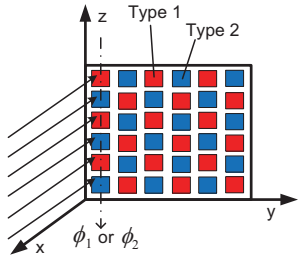


Fig. 4. The chessboard-like design of the reflect-array.

(*length* × *height* × *thickness*). There are  $14 \times 16 = 224$  reflector units on the panel in total. Therefore, the distance between two adjacent patches is designed to be longer than one wavelength to prevent the patches from coupling.

For the reflector unit design, the basic idea is to load microstrip patches with electronically-controlled relay switches. As shown in Fig. 3, each reflector unit is controlled by an Omron G6L-1P-DC5 relay switch. When the switch is open, the patch is isolated from the ground plane. Therefore, the patch is turned “on” and becomes a resonant reflector that has the maximum reflection for 60 GHz signals. Once the switch is closed, the patch is shorted by the ground plane and transitions to the “off” status that has the minimum reflection. Hence, each element on the reflect-array can be turned on or off to reflect the incident signals.

As shown in Fig. 4, two types of rectangular reflectors with different patch lengths are deployed as a chessboard on the panel. The dimensions of Type 1 and Type 2 patches are  $5.1 \text{ mm} \times 4.65 \text{ mm}$  and  $5.1 \text{ mm} \times 4.95 \text{ mm}$ , respectively. The full wave simulation using COMSOL multiphysics [21] in Fig. 5 shows that both types of patches have high radar-cross-section

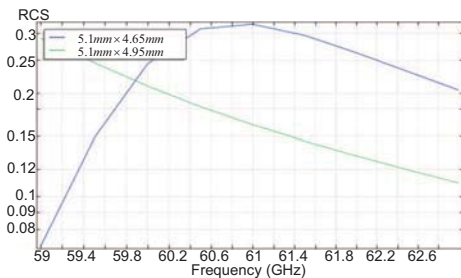


Fig. 5. The RCS of the reflectors.

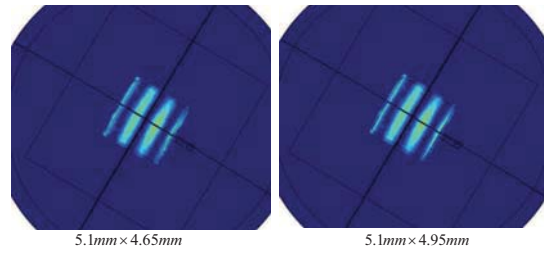


Fig. 6. The energy distribution on the patches.

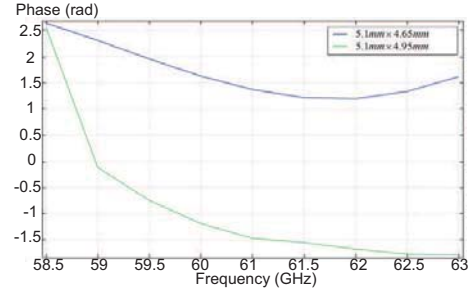


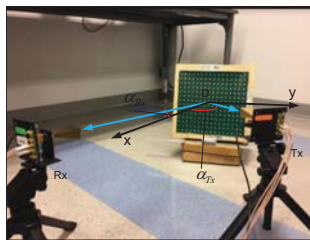
Fig. 7. The phase control of reflectors.

(RCS) over 0.2 around 60 GHz. As shown in Fig. 6, with 60 GHz incident waves, a high energy distribution shown by light blue can be obtained on the two edges of the patches. This simulation result further demonstrates that the resonance can be obtained around 60 GHz. Since two types of patches have different patch lengths, the board can provide different phase controls  $\phi_1$  and  $\phi_2$  that  $|\phi_1 - \phi_2| \approx \pi$  around 60 GHz as shown in Fig. 7. This chessboard-like design is used to provide two different phase controls for the reflected signals. Considering an incident plane-wave signal from the transmitter in the  $x$ - $y$  plane as illustrated in Fig. 4, the signal propagation direction is orthogonal to the  $z$ -axis. For each column of patches, either Type 1 patches or Type 2 patches can be turned “on” to provide a phase control of  $\phi_1$  or  $\phi_2$ . Therefore, the reflected signal can be steered towards any directions in the  $x$ - $y$  plane.

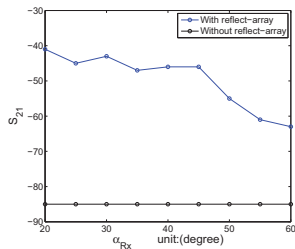
### C. Experimental Evaluation

To validate the proposed system, we use a test-bed shown in Fig. 8. The transceivers are deployed in front of the reflect-array to measure the strength of the reflected signals. In this test-bed, the relay switches are controlled by MEGA 2560 micro-controllers. The mmWave transceivers are realized by the VubIQ development system [22] and the horn antennas with 8-degree beam-width as shown in Fig. 9(a). The network analyzer is used for the signal generation and observation.

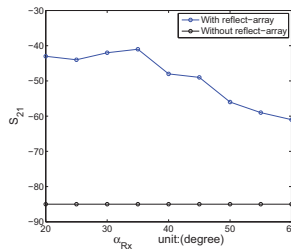
As shown in Fig. 9(a), the reflect-array panel is located orthogonal to the  $x$ -axis. The transceivers and the center of the reflect-array are deployed on the  $x$ - $y$  plane. Shown as blue arrows, the distances between the transceivers and the center of the reflect-array are 0.5m (Tx) and 1m (Rx). The intersection angle between the  $x$ -axis and the direction vector of the transmitter is  $\alpha_{Tx}$ , and the angle for the receiver is  $\alpha_{Rx}$ . As shown in Fig. 9(b), the transmitter is deployed on the  $x$ -axis so that  $\alpha_{Tx} = 0^\circ$ . The reflect-array is controlled to beamform



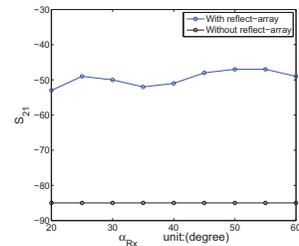
(a) The setup of the experiment.



(b) Incident angle = 0 degree.



(c) Incident angle = 30 degree.



(d) Incident angle = 60 degree.

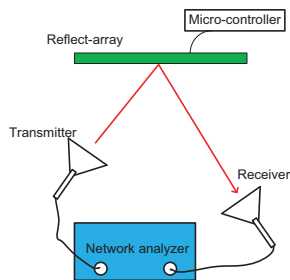
 Fig. 9. The experimental setup and  $S_{21}$  measurements.


Fig. 8. The test-bed for proof-of-concept experiments.

the signal from  $\alpha_{Rx} = 20^\circ$  to  $\alpha_{Rx} = 60^\circ$  with a step of  $5^\circ$ . The details of the control algorithm are presented in Section III A. In this experiment, the ratio of the transmitted power to the received power is measured and denoted as  $S_{21}$ . The blue curve in Fig. 9(b), 9(c), and 9(d) are  $S_{21}$  measured at each beam direction and the black curve is the  $S_{21}$  measured in the absence of a reflect-array. When no reflect-array is present, the signal becomes extremely low and only noise at  $-85\text{dB}$  is received. Similarly, the transmitter is moved to  $\alpha_{Tx} = 30^\circ, 60^\circ$  and the experimental results are shown as Fig. 9(c) and Fig. 9(d), respectively. The two curves on each figure show the significant enhancement of the received power thanks to the beamforming from the reflect-array.

### III. REFLECT-ARRAY CONTROL AND BEAM-SEARCHING ALGORITHM

To bypass the obstacles and establish communication links between the transceivers, the smart reflect-array needs to be optimally controlled to find the desired receiver. In the reflect-array-assisted 802.11ad networks, the reflect-array reflects the incident signal during the beam-searching phase of the AP. However, since there are multiple users to be served and the users may be mobile, the reflect-array does not know the position of the desired user. In this section, we first model the mmWave channel with the reflect-array involved. Based on the channel model, the reflect-array control algorithm is developed. Then, a basic idea of the beam-searching algorithm is presented and we leave the detailed system design as the future work.

#### A. Reflect-array Control Algorithm

Once the reflection occurs on the reflect-array, the signal received at the user is the superposition of the multi-path sig-

nals reflected on the reflector units. Hence, the received signal strongly depends on the phases of the multi-path propagation. Assuming that the signal transmitted on baseband is a train of raised cosines bearing BPSK symbols  $m(t)$ , the received signal reflected from the reflect-array can be expressed in the time domain as:

$$r(t) = m(t)e^{j2\pi f_c} \sum_{i=1}^N a_i e^{-j(\theta_i - \varphi_i)} + n(t), \quad (1)$$

where  $f_c$  is the operating frequency,  $a_i$ ,  $\theta_i$  are the attenuation and phase shift of the  $i$ -th path, respectively,  $\varphi_i$  is the phase induced by the  $i$ -th reflector for all  $i = 1, 2, \dots, N$ ,  $n(t)$  is the noise component of the received signal. Since the received signal consists of the signal from the source and the noise, whether the communication can be established or not depends on the signal-to-noise ratio (SNR). The SNR at the receiver can be expressed as:

$$SNR = \frac{\rho^2 |\mathbf{h}^H \mathbf{v}_\varphi|^2}{\sigma^2}, \quad (2)$$

where

$$\mathbf{h} \triangleq [a_1 e^{j\theta_1} \quad a_2 e^{j\theta_2} \dots \quad a_N e^{j\theta_N}]^T, \quad \rho^2 \triangleq E\{|m(t)|^2\}, \quad (3)$$

$$\mathbf{v}_\varphi \triangleq [e^{j\varphi_1} \quad e^{j\varphi_2} \dots \quad e^{j\varphi_N}], \quad \sigma^2 \triangleq E\{|n(t)|^2\}.$$

Since the reflectors can provide large enough bandwidth for communication, the received spectrum is almost flat on the frequency band. Hence, the SNR can be represented as (2) regardless of the modulation scheme. Therefore, the phase control can be formulated as an optimization problem:

$$\begin{aligned} & \max_{\mathbf{v}_\varphi} SNR, \\ & s.t. \quad \varphi_i \in [0, 2\pi), \forall i = 1, 2, \dots, N. \end{aligned} \quad (4)$$

Obviously, the optimal control is to harmonize the phases at the receiver side so that the dominating factor  $|\mathbf{h}^H \mathbf{v}_\varphi|$  in (2) can be maximized. For the traditional beamforming based on the reflect-array, the control algorithm can be expressed as:

$$\varphi_i = k_0 \left( |\vec{r}_i - \vec{r}_{AP}| + \vec{r}_i \cdot \vec{u} \right) \bmod 2\pi, \quad (5)$$

where  $k_0$  is the wave number. As shown in Fig. 10(a),  $\vec{r}_i$  is the position vector of the  $i$ -th reflector unit,  $\vec{r}_{AP}$  is that of the AP, and  $\vec{u}$  is the unit vector of the required beam direction. The phase control  $\varphi_i$  is obtained by the modulo operation to make it between 0 and  $2\pi$ .

Different from the traditional beamforming reflect-array, the

reflect-array for mmWave signals needs variable capacitors with very low capacitance (smaller than  $0.1pF$ ) to continuously tune the phase response of reflector units. Due to this hardware limitation, instead of continuous phase control, binary phase control can be utilized according to the quantization method in [17]:

$$\varphi_{binary,i} = \begin{cases} \phi_1, & 0 \leq \varphi_i < \pi, \\ \phi_2, & \pi \leq \varphi_i < 2\pi. \end{cases} \quad (6)$$

Theoretically, the quantization of the phase control in (6) causes the SNR loss. However, the quantization is not the dominant cause of SNR loss in practice. Due to the short wavelength of the signal, high-accuracy phase control is required to perfectly align the phases on the beam form direction. With the initial design, the hardware limitation causes significant SNR loss.

As shown in Fig. 10(b), based on the chessboard-like design introduced in Section II B, each column of patches can provide either  $\phi_1$  or  $\phi_2$  phase control. Therefore, the reflected signals have the same signs of phases and enhance each other on the required beam direction.

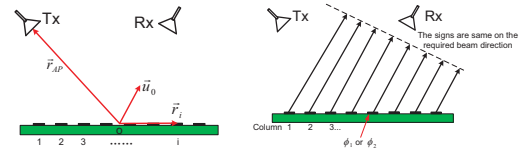
### B. The Beam-Searching Algorithm for Desired Users

Since the position of the user is unknown, the beam-searching algorithm is required. Here, we describe an algorithm consisting of two phases. At the first phase, the reflect-array roughly trains beamforming directions as shown in Fig. 11(a). According to the 802.11ad protocol, the AP searches for the desired user by beamforming the transmitting signal to sweep Sector 1, Sector 2, ..., Sector  $M$ , successively. A physical control link using Wi-Fi or Bluetooth can be established between the reflect-array and the AP to concert the beam searching of the reflect-array. At the beginning, the reflect-array keeps reflecting the signal towards an arbitrary direction  $\vec{u}_k \in \{\vec{u}_1, \vec{u}_2, \dots, \vec{u}_K\}$ . Once the AP reaches the Sector  $m$  during the beam-searching process from Sector 1 to Sector  $M$ , the signal reaches the reflect-array and then is reflected along  $\vec{u}_k$ . At this time, the beam pair of the AP and the reflect-array is denoted by  $\{1, \vec{u}_k\}$ . However, since the user is not located on the direction of  $\vec{u}_k$ , the user cannot hear from the AP to establish the link. Therefore, once the AP starts the second round of the beam-searching from Sector 1 to Sector  $M$ , the reflect-array switches to the next beamforming direction  $\vec{u}_{k+1}$ . Therefore, once the AP finishes a round of beam-searching, the reflect-array switches to the next state until the link is established by the beam pair  $\{m, \vec{u}^*\}$ . Respectively denoting the duration of each control status of the AP and the reflect-array by  $T_{AP}$  and  $T_r$ , we have the following relationship:

$$T_r = MT_{AP}. \quad (7)$$

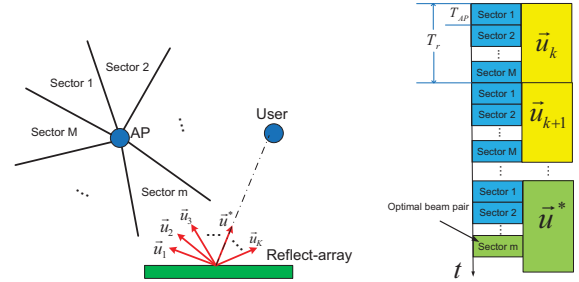
This relationship can be illustrated as the schedule in Fig. 11(b).

The communication link can be established by the solution  $\vec{u}^*$  obtained from the first phase. However, since the resolution of the searching step is not high enough in the first phase, the user may not be located on the direction of  $\vec{u}^*$ . Therefore,  $\vec{u}^*$  may not be the optimal beam direction and further adjustment might be necessary during the communication as the second stage of the beam-searching.



(a) The position and unit vectors. (b) The binary phase control.

Fig. 10. The position vectors and binary phase control



(a) The beam-searching of the AP and (b) The schedule of the reflect-array.

Fig. 11. The beam-searching at the first stage.

Give an initial solution  $\mathbf{a}^{(0)} = \vec{u}^* = (x^{(0)}, y^{(0)})$  obtained from the first stage of the beam-searching, two searching directions are defined as:

$$\mathbf{d}^{(0)+} = (-y^{(0)}, x^{(0)}), \quad \mathbf{d}^{(0)-} = (y^{(0)}, -x^{(0)}). \quad (8)$$

$\mu > 1$  and  $-1 < \nu < 0$  are defined as the magnification factor and shrinkage factor, respectively. Starting from the initial solution, we first search along  $\mathbf{d}^{(0)+} = (-y^{(0)}, x^{(0)})$ . Considering that  $g(\cdot)$  is the SNR measured at the user side for the beam direction “.” in real time, the movement is successful if  $g(\mathbf{a}^{(0)} + \lambda^{(0)}\mathbf{d}^{(0)+}) \geq g(\mathbf{a}^{(0)})$  is held. Therefore, we have:

$$\mathbf{a}^{(1)} = \begin{cases} \frac{\mathbf{a}^{(0)} + \lambda^{(0)}\mathbf{d}^{(0)+}}{\|\mathbf{a}^{(0)} + \lambda^{(0)}\mathbf{d}^{(0)+}\|}, & \text{if } g(\mathbf{a}^{(0)} + \lambda^{(0)}\mathbf{d}^{(0)+}) \geq g(\mathbf{a}^{(0)}), \\ \mathbf{a}^{(0)}, & \text{otherwise,} \end{cases} \quad (9)$$

where  $\lambda^{(0)}$  is the proper searching step. Once the new solution  $\mathbf{a}^{(1)}$  is calculated, the searching step is updated by:

$$\lambda^{(1)} = \begin{cases} \mu\lambda^{(0)}, & \text{if } g(\mathbf{a}^{(0)} + \lambda^{(0)}\mathbf{d}^{(0)+}) \geq g(\mathbf{a}^{(0)}), \\ \nu\lambda^{(0)}, & \text{otherwise.} \end{cases} \quad (10)$$

According to (10), if the movement is successful, a larger movement is needed in the next round of searching. Otherwise, a back-off search should be adopted in the next round. After searching along the direction  $\mathbf{d}^{(0)+}$ , the similar searching operations is used on the other direction  $\mathbf{d}^{(0)-}$ . Then, the first round searching is completed and the second round begins from the new beam direction  $\mathbf{a}^{(1)}$ . Given an existing beam direction  $\mathbf{a}^{(n)} = (x^{(n)}, y^{(n)})$ , the searching directions are updated as well:

$$\mathbf{d}^{(n)+} = (-y^{(n)}, x^{(n)}), \quad \mathbf{d}^{(n)-} = (y^{(n)}, -x^{(n)}). \quad (11)$$

Finally, the second stage of beam-searching stops once the relative change of the adjacent solutions drops below a threshold:

$$\|\mathbf{a}^{(n+1)} - \mathbf{a}^{(n)}\| \leq \eta. \quad (12)$$

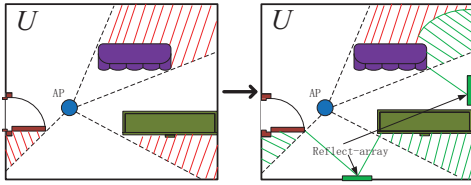


Fig. 12. The signal coverage in the room.

#### IV. THE DEPLOYMENT OF THE SMART REFLECT-ARRAY

Since the reflect-array is used as a smart mirror to let the signals from the AP bypass the obstacles via reflections, the deployment of the reflect-array significantly affects the AP coverage. In practice, a deployment strategy requires the knowledge of the floor layout, which in many cases is difficult if impossible to obtain. In this section, we propose a basic principle of reflect-array deployment based on the mathematical model of the indoor signal coverage. The objective of the deployment principle is to minimize the outage probability of the mmWave communication links. Based on this principle, practical guidelines of the reflect-array deployment can be developed in future work.

As shown on the left side of Fig. 12, the AP is deployed in a room of area of  $U$ . Due to the blockage from the obstacle, the signals from the AP can only cover the area  $A_0$  shown as the white area in the room. The red shadow area indicates the blocked area that is not covered by the signals. Once the reflect-arrays are deployed on the walls, the signal coverage is enlarged to  $A = A_0 \cup A_1(\mathbf{p}_r)$  shown as the right side of Fig. 12.  $A_1(\mathbf{p}_r)$  is the additional signal coverage area shown as the green shadow area. Obviously,  $A_1$  is strongly related to  $\mathbf{p}_r$  which varies if the position of the reflect-array is changed.

For a certain user's location  $\mathbf{p}_u$ , the connection probability that a link can be successfully established is expressed as:

$$P_{cn} = P(\mathbf{p}_u \text{ is in } A) \cdot P(SNR \geq \beta | \mathbf{p}_u \text{ is in } A), \quad (13)$$

where  $\beta$  is the threshold for the SNR to establish the communication link. According to (2), if the reflect-array is optimally controlled, the maximum SNR can be calculated as:

$$SNR_{max} = \frac{c\rho^2}{(1+d)^\alpha \sigma^2}, \quad (14)$$

where  $d$  is the propagation length from the AP to the user,  $c$  is the reflection coefficient of the reflect-array, and  $\alpha$  indicates the decay of the signal with the distance increase. If the position of the users follows a certain distribution, the probability of a user being located at  $\mathbf{p}_u$  can be written as  $f(\mathbf{p}_u)ds$ , where  $f(\mathbf{p}_u)$  is the PDF of  $\mathbf{p}_u$  determined by the distribution of the users in  $U$ , and  $ds$  is the infinitesimal element of the area located at  $\mathbf{p}_u$ . Therefore, if the position of the AP  $\mathbf{p}_{AP}$  is fixed, the connection probability can be calculated as:

$$P_{cn} = \int_{A_0} F\left(\frac{c\rho^2}{[1+d_0(\mathbf{p}_u)]^\alpha \sigma^2}\right) f(\mathbf{p}_u)ds + \int_{A_1(\mathbf{p}_r)} F\left(\frac{c\rho^2}{[1+d(\mathbf{p}_r, \mathbf{p}_u)]^\alpha \sigma^2}\right) f(\mathbf{p}_u)ds, \quad (15)$$

where  $d_0(\mathbf{p}_u)$ ,  $d(\mathbf{p}_r, \mathbf{p}_u)$  are respectively the signal propagation lengths of the direct path and the reflected path through the

reflect-array:

$$d_0(\mathbf{p}_u) = \|\mathbf{p}_{AP} - \mathbf{p}_u\|, \quad (16)$$

$$d(\mathbf{p}_r, \mathbf{p}_u) = \|\mathbf{p}_{AP} - \mathbf{p}_r\| + \|\mathbf{p}_r - \mathbf{p}_u\|.$$

The  $F(x)$  in (15) is the indicator function developed as:

$$F(x) = \begin{cases} 1, & x \geq \beta, \\ 0, & x < \beta. \end{cases} \quad (17)$$

According to (15), the result can be extended by considering multiple reflect-arrays:

$$P_{cn,L} = \int_{A_0} F\left(\frac{c\rho^2}{[1+d_0(\mathbf{p}_u)]^\alpha \sigma^2}\right) f(\mathbf{p}_u)ds + \sum_{i=1}^L \int_{A_1(\mathbf{p}_{ri}) - \cup_{j \neq i} A_1(\mathbf{p}_{rj})} F\left(\frac{c\rho^2}{[1+d(\mathbf{p}_{ri}, \mathbf{p}_u)]^\alpha \sigma^2}\right) f(\mathbf{p}_u)ds + \sum_{n=1}^{N(b_n)} \int_{b_n} \left\{ 1 - \prod_{i \in C_v(b_n)} \left[ 1 - F\left(\frac{c\rho^2}{[1+d(\mathbf{p}_{ri}, \mathbf{p}_u)]^\alpha \sigma^2}\right) \right] \right\} f(\mathbf{p}_u)ds, \quad (18)$$

where  $L$  is the number of reflect-arrays, and  $i, j$  denote the  $i$ -th and  $j$ -th deployed reflect-array, respectively. Since an area may be covered by multiple reflect-arrays, we denote as  $b_n$  the  $n$ -th overlapped area.  $N(b_n)$  is the number of overlapped areas.

Therefore, the optimal deployment of the reflect-arrays can be calculated by minimizing the outage probability of the communication links:

$$\min_{\mathbf{p}_{ri}} P_{ot,L}, \quad (19)$$

$$s.t. \quad \mathbf{p}_{ri} \in D, \forall i = 1, 2, \dots, L,$$

where  $D$  is the set of reflect-array deployment positions on the wall of a room.  $P_{ot,L}$  is the outage probability calculated by  $P_{ot,L} = 1 - P_{cn,L}$ .

Then we consider that the movement of the user follows the individual mobility model according to [20]:

$$P_{new}(n) = \xi S^{-\gamma}(n), \quad P_{rt}(n) = 1 - P_{new}(n), \quad (20)$$

where  $P_{new}(n)$ ,  $P_{rt}(n)$  are respectively the probability of visiting a new position and the probability of visiting an old position.  $0 < \xi \leq 1$  and  $\gamma > 0$  are parameters related to the user's mobility habits.  $S(n)$  is the number of visited positions in  $n$  jumps and  $n$  is the jump number. Therefore, the probability that the user departure the signal coverage area is expressed as:

$$P_d = 1 - \left\{ \frac{1}{\bar{v}} \left[ \left( \frac{A}{U} \right)^2 E[d_{i,i}] + \left( 1 - \frac{A}{U} \right) \frac{A}{U} E[d_{o,i}] \right] + \frac{A}{U} E[\Delta t_i] \right\} / \left\{ \frac{1}{\bar{v}} \left[ \left( \frac{A}{U} \right)^2 E[d_{i,i}] + 2 \left( 1 - \frac{A}{U} \right) \frac{A}{U} E[d_{o,i}] + \left( 1 - \frac{A}{U} \right)^2 \right] + \frac{A}{U} E[\Delta t_i] + \left( 1 - \frac{A}{U} \right) E[\Delta t_o] \right\}, \quad (21)$$

where  $\Delta t_i$  is the waiting time inside the signal coverage area that follows  $f(\Delta t_i) = |\Delta t_i|^{-1-\beta_i}$ ,  $0 < \beta_i \leq 1$ .  $\Delta t_o$  is the waiting time outside the signal coverage area that follows  $f(\Delta t_o) = |\Delta t_o|^{-1-\beta_o}$ ,  $0 < \beta_o \leq 1$ .  $d_{i,i}$  is the distance between two points inside the signal coverage area, and  $d_{o,o}$  is that of outside.  $d_{o,i}$  is the distance between one point inside and another point outside the signal coverage area.  $\bar{v}$  is the average

velocity of the user. For a mobile user, if the communication link is required to be established in time, the user needs to be located in the signal coverage area at the beginning. In addition, the user should not depart the signal coverage area during the movement to complete the communication. Therefore, by considering a mobile user, the probability that a link can be established and maintained is calculated according to (18) and (21):

$$P_{cn,L,m} = (1 - P_d)P_{cn,L}. \quad (22)$$

An outage occurs if the user's position is outside the signal coverage area during the movement. Therefore, the optimal deployment of the reflect-arrays is obtained by minimizing the outage probability:

$$\begin{aligned} \min_{\mathbf{p}_{ri}} \quad & P_{ot,L,m}, \\ \text{s.t.} \quad & \mathbf{p}_{ri} \in D, \forall i = 1, 2, \dots, L, \end{aligned} \quad (23)$$

where  $P_{ot,L,m}$  is the outage probability by considering mobile users calculated by  $P_{ot,L,m} = 1 - P_{cn,L,m}$ .

Then we consider that both the user and the obstacle are mobile. In this case,  $E[d_{i,i}]$ ,  $E[d_{i,o}]$ ,  $E[d_{o,o}]$ , and the movement of the obstacles  $A$  become time-varying and the movement of the obstacles is independent from the user's movement. The expectations of these parameters are then calculated by:

$$\begin{aligned} E[A(t)] &= \frac{1}{t_m} \int_0^{t_m} A(t) dt, & E[\bar{d}_{i,i}(t)] &= \frac{1}{t_m} \int_0^{t_m} \bar{d}_{i,i}(t) dt, \\ E[\bar{d}_{i,o}(t)] &= \frac{1}{t_m} \int_0^{t_m} \bar{d}_{i,o}(t) dt, & E[\bar{d}_{o,o}(t)] &= \frac{1}{t_m} \int_0^{t_m} \bar{d}_{o,o}(t) dt, \end{aligned} \quad (24)$$

where the communication is considered within a duration of  $t_m$ .  $\bar{d}_{i,i}(t)$ ,  $\bar{d}_{i,o}(t)$ , and  $\bar{d}_{o,o}(t)$  indicate the average distances at time  $t$ . Hence, the probability that the user pauses in the signal coverage area by considering obstacles' movement can be calculated as:

$$\begin{aligned} P_{p,m} &= \left\{ \frac{1}{v} \left[ Z^2 E[\bar{d}_{i,i}] + (1 - Z) ZE[\bar{d}_{o,i}] \right] + ZE[\Delta t_i] \right\} \\ & / \left\{ \frac{1}{v} \left[ ZE[\bar{d}_{i,i}] + 2(1 - Z) ZE[\bar{d}_{o,i}] + (1 - Z)^2 \right] \right. \\ & \left. + ZE[\Delta t_i] + (1 - Z) E[\Delta t_o] \right\}, \end{aligned} \quad (25)$$

where  $Z = \frac{E[A(t)]}{U}$ . Therefore, by considering the mobile user and obstacles, the probability that a link can be established and maintained can be written as:

$$P_{cn,L,2m} = P_{p,m} P_{cn,L}. \quad (26)$$

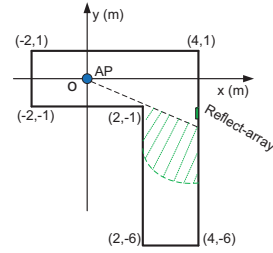
The optimal deployment of the reflect-arrays can be obtained by solving:

$$\begin{aligned} \min_{\mathbf{p}_{ri}} \quad & P_{ot,L,2m}, \\ \text{s.t.} \quad & \mathbf{p}_{ri} \in D, \forall i = 1, 2, \dots, L, \end{aligned} \quad (27)$$

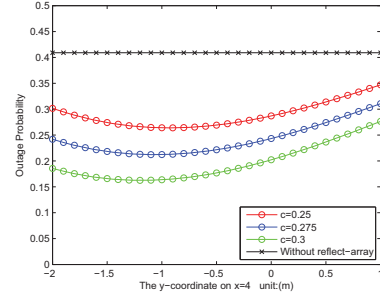
where  $P_{ot,L,2m} = 1 - P_{cn,L,2m}$ .

## V. NUMERICAL ANALYSIS OF THE OUTAGE PROBABILITY

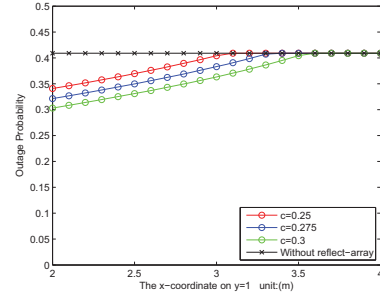
In this section, we evaluate the outage probability of the communication links by optimally deploying the reflect-arrays in different indoor scenarios based on the analysis presented in Section IV. In this numerical analysis, the transmitting



(a) The deployment of the reflect-array.



(b) The outage probability by deploying the reflect-array on  $x=4$ .



(c) The outage probability by deploying the reflect-array on  $y=1$ .

Fig. 13. The deployment and outage evaluation in a turning.

power from the AP is set to 3 dBm and the noise level is -90dBm. The threshold for the SNR is assumed to be 60 dB. According to the simulation result of the reflector unit, the reflection coefficient  $c$  varies from 0.2 to 0.3 around 60 GHz frequency band. Therefore, in this section, we evaluate the outage probability by considering  $c = 0.2, 0.25, 0.3$ .

Fig. 13(a) shows the floorplan of an aisle. The AP is located at the origin of the coordinate system and the positions of users follow the uniform distribution in the aisle. The walls are considered as the boundary that cannot reflect the signal to the desired user. Obviously, the signal from the AP can cover the horizontal branch of the aisle but cannot propagate to most of the area in the vertical branch due to the blockage of the turning. As a result, the communication outage occurs if the user is located in the vertical branch far away from the turning. Therefore, the reflect-array is deployed on the wall  $x = 4$  or  $y = 1$  to enlarge the signal coverage shown as the green

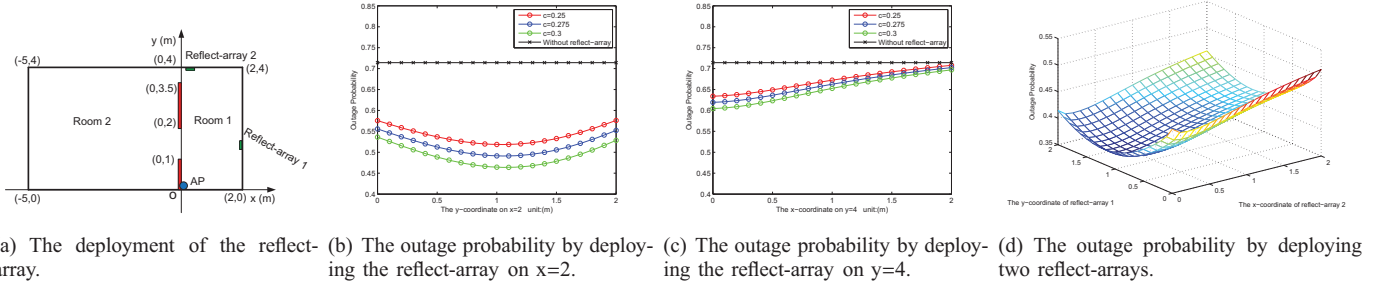


Fig. 14. The deployment and outage evaluation in the rooms.

dashed area. We first analyze the deployment on  $x = 4$  shown as Fig. 13(b). The  $x$ -axis is the  $y$ -coordinate of the reflect-array on  $x = 4$  and the  $y$ -axis is the outage probability. The  $y$ -coordinate of the reflect-array is searched from  $-2$  to  $1$  with a step of  $0.1$ . Shown as the black curve, the outage probability without using the reflect-array is fixed at  $0.41$ . We use a black horizontal line in the figure since the outage probability is not related to the reflect-array in this case. The outage probability significantly decreases as the reflection coefficient  $c$  increases. Similarly, we evaluate the outage probability by deploying the reflect-array on  $y = 1$  in Fig. 13(b). As a conclusion, the optimal deployment of the reflect-array is  $(4, -1.2)$  and the outage probability reduces to  $0.16$  if the reflection coefficient is  $0.3$ .

As shown in Fig. 14(a), we evaluate the outage probability by considering the AP deployed at the origin in the rooms. Due to the blockage from the obstacles between room 1 and room 2 shown as the red bars, the signal can only cover room 1. By deploying a reflect-array on  $x = 2$  or  $y = 4$ , the outage probability significantly decreases as shown in Fig. 14(b) and Fig. 14(c) since the reflect-array can beamform the signal to cover more area in room 2. As a conclusion, the optimal position for the reflect-array is  $(2, 1.1)$  and the outage probability drops from  $0.71$  to  $0.47$  if  $c = 0.3$ . As shown in Fig. 14(d), we evaluate the outage probability by deploying two reflect-arrays on  $x = 2$  and  $y = 4$ . Considering the reflection coefficient  $c = 0.3$ , the outage probability drops to  $0.37$  with the optimal solution that reflect-arrays 1, 2 are located at  $(2, 1.2)$  and  $(0.2, 4)$ , respectively.

The outage probability for the mobile user is evaluated in Fig. 15. As shown in Fig. 15(a), the AP is located at the origin and the signal can only cover the right side of the room. A mobile user is moving in the room with an average velocity  $\bar{v} = 0.1m/s$  and  $\bar{v} = 0.2m/s$ . In this evaluation, the parameters  $\beta_i = 0.5$  and  $\beta_o = 1.5$ . We first evaluate the deployment on  $x = 2$  as shown in Fig. 15(b). By deploying the reflect-array at  $y = 1.5$ , the outage probability decreases to  $0.49$  if  $\bar{v} = 0.1m/s$ . Shown in Fig. 15(c), the outage probability can be further reduced to  $0.17$  if the reflect-array is deployed at  $(0, 4)$ . Then we evaluate the outage probability by adding a mobile obstacle shown in Fig. 16(a). The obstacle with 1-meter length is deployed vertically to the  $x$ -axis. At the beginning, the center of the obstacle is located at  $(-1, 3.5)$  and it moves to  $(-1, 0.5)$  along  $x = -1$  with the constant velocity. As shown

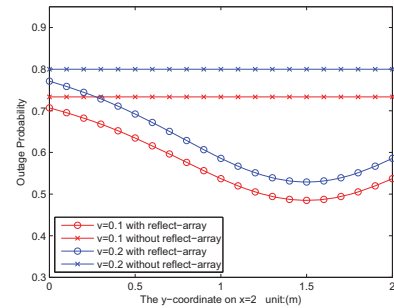
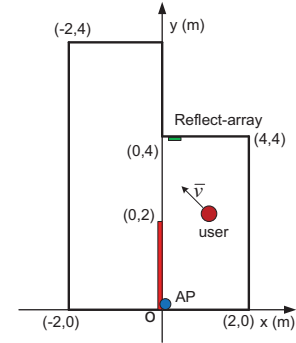
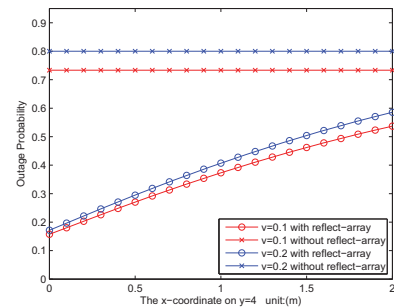
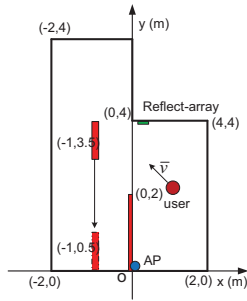
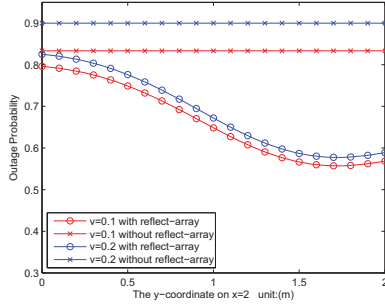

 (b) The outage probability by deploying the reflect-array on  $x=2$ .

 (c) The outage probability by deploying the reflect-array on  $y=4$ .

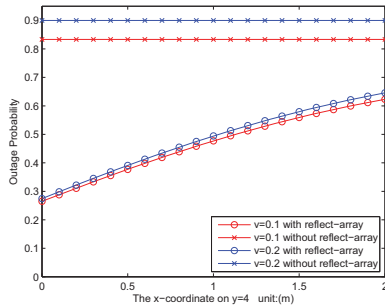
Fig. 15. The deployment and outage evaluation for the mobile user.



(a) The deployment of the reflect-array.



(b) The outage probability by deploying the reflect-array on  $x=2$ .



(c) The outage probability by deploying the reflect-array on  $y=4$ .

Fig. 16. The deployment and outage evaluation for the mobile user and obstacle.

in Fig. 16(b) and 16(c), the outage probability is evaluated by deploying the reflect-array on  $x = 2$  and  $y = 4$ , respectively. Due to the blockage from the moving obstacle, the outage probability is larger than that in Fig. 15. The result in Fig. 16(c) shows that the optimal position is  $(0, 4)$ . The outage probability decreases to 0.26 for  $\bar{v} = 0.1\text{m/s}$ .

## VI. CONCLUSION

In this paper, a smart reflect-array is developed to solve the problem of signal blockage in mmWave indoor communications. We successfully demonstrate the solution by in-lab test-bed experiments. The experimental result shows that the developed reflect-array can steer the incident signal towards the desired receiver to establish the robust link between the transceivers. Then, we develop a two-stage beam-searching

algorithm to accurately determine the required beam direction for the desired users. To adequately utilize the smart reflect-array in the indoor environments, we analyze the reflect-array deployment by considering the mobile users and environments. Finally, the reflect-array deployment and the outage probability of the communication link are evaluated via numerical analysis.

## REFERENCES

- [1] R. H. Tehrani, S. Vahid, D. Triantafyllopoulou, H. Lee, and K. Moessner, "Licensed Spectrum Sharing Schemes for Mobile Operators: A Survey and Outlook," *IEEE Communications Survey & Tutorials*, vol. 18, No. 4, pp. 2591-2623, June, 2016.
- [2] X. Wang, T. Q. S. Quek, M. Sheng, and J. Li, "Throughput and Fairness Analysis of Wi-Fi and LTE-U in Unlicensed Band," *IEEE Journal on Selected Areas in Communications*, vol. 35, No. 1, pp. 63-78, January, 2017.
- [3] Z. Pi and F. Khan, "An Introduction to Millimeter-Wave Mobile Broadband Systems," *IEEE Communications Magazine*, vol. 49, No. 6, pp. 101-107, June, 2011.
- [4] L. Wei, R. Q. Hu, Y. Qian, and G. Wu, "Key Elements to Enable Millimeter Wave Communications for 5G Wireless Systems," *IEEE Wireless Communications*, vol. 21, No. 6, pp. 136-143, December, 2014.
- [5] T. S. Pappaport et al, "Millimeter Wave Mobile Communications for 5G Cellular: It Will Work!" *IEEE Access*, vol. 1, pp. 335-349, May, 2013.
- [6] D. Lockie and D. Peck, "High-data-rate millimeter-wave radios," *IEEE Microwave Magazine*, vol. 10, No. 5, pp. 75-83, July, 2009.
- [7] IEEE 802.11 Task Group AD, "IEEE 802.11ad, Amendment 3: Enhancements for Very High Throughput in the 60 GHz Band", 2012.
- [8] K. Haneda, J. Jarvelainen, A. Karttunen, M. Kyro, and J. Putkonen, "A Statistical Spatio-Temporal Radio Channel Model for Large Indoor Environments at 60 and 70 GHz," *IEEE Transactions on Antennas and Propagation*, vol. 63, No. 6, pp. 2694-2704, June, 2015.
- [9] G. R. Maccartney, T. S. Rappaport, S. Sun, and S. Deng, "Indoor Office Wideband Millimeter-Wave Propagation Measurements and Channel Models at 28 and 73 GHz for Ultra-Dense 5G Wireless Networks," *IEEE Access*, vol. 3, pp. 2388-2424, October, 2015.
- [10] H. Jung and I. Lee, "Outage Analysis of Millimeter-Wave Wireless Backhaul in the Presence of Blockage," *IEEE Communications Letters*, vol. 20, No. 11, pp. 2268-2271, August, 2016.
- [11] J. Qiao, X. Shen, J. W. Mark, and L. Lei, "Video Quality Provisioning for Millimeter Wave 5G Cellular Networks With Link Outage," *IEEE Transactions on Wireless Communications*, vol. 14, No. 10, pp. 5692-5703, June, 2015.
- [12] O. Abari, D. Bharadia, A. Duffield, and D. Katabi, "Enabling High-quality Untethered Virtual Reality," in *Proc. 14th USENIX Symposium on Networked Systems Design and Implementation*, Boston, USA, March, 2017.
- [13] W. Roh, J. Seol, J. Park, B. Lee, J. Lee, Y. Kim, J. Cho, and K. Cheun, "Millimeter-Wave Beamforming as an Enabling Technology for 5G Cellular Communications: Theoretical Feasibility and Prototype Results," *IEEE Communications Magazine*, vol. 52, No. 2, pp. 106-113, February, 2014.
- [14] B. Li, Z. Zhou, W. Zou, X. Sun, and G. Du, "On the Efficient Beam-Forming Training for 60GHz Wireless Personal Area Networks," *IEEE Transactions on Wireless Communications*, vol. 12, No. 2, pp. 504-515, February, 2013.
- [15] R. W. Heath, N. Gonzalez-Prelcic, S. Rangan, W. Roh, and A. M. Sayeed, "An Overview of Signal Processing Techniques for Millimeter Wave MIMO Systems," *IEEE Journal of Selected Topics in Signal Processing*, vol. 10, No. 3, pp. 436-453, April, 2016.
- [16] X. Zhou, Z. Zhang, Y. Zhu, Y. Li, S. Kumar, A. Vahdat, B. Y. Zhao, and H. Zheng, "Mirror Mirror on The Ceiling: Flexible Wireless Links for data Centers," in *Proc. ACM SIGCOMM Computer Communication Review*, vol. 42, No. 4, October, 2012.
- [17] H. Kamoda, T. Iwasaki, J. Tsumochi, T. Kuki, and O. Hashimoto, "60-GHz Electronically Reconfigurable Large Reflectarray Using Single-Bit Phase Shifters," *IEEE Transactions on Antennas and Propagation*, vol. 59, No. 7, pp. 2524-2531, July, 2011.
- [18] T. Nitché, A. B. Flores, E. W. Knightly, and J. Widmer, "Steering with Eyes Closed: mm-Wave Beam Steering without In-Band Measurement," in *Proc. IEEE Conference on Computer Communications (INFOCOM)*, Hong Kong, China, April, 2015.
- [19] S. Sur, V. Venkateswaran, X. Zhang, and P. Ramanathan, "60 GHz Indoor Networking through Flexible Beams: A Link-Level Profiling," in *Proc. ACM International Conference on Measurement and Modeling of Computer System (SIGMETRICS)*, Portland, USA, June, 2015.
- [20] X. Ge, J. Ye, Y. Yang, and Q. Li, "User Mobility Evaluation for 5G Small Cell Networks Based on Individual Mobility Model," *IEEE Journal on Selected Areas in Communications*, vol. 34, No. 3, pp. 528-541, March, 2016.
- [21] [Online]. Available: <http://www.comsol.com>
- [22] [Online]. Available: <http://www.vubiqnetworks.com>